AIAA JOURNAL
Vol. 47, No. 1, January 2009

Dimensional Stability Testing on a Space Optical Bench Structure

Ruben Edeson* and Nigel Morris*
Rutherford Appleton Laboratory, Chilton, England OX11 0QX, United Kingdom
and
Adrian Tatnall† and Guglielmo S. Aglietti†
University of Southampton, Southampton, England SO17 1BJ, United Kingdom

DOI: 10.2514/1.38228

High-performance space-based optical systems typically require structures that exhibit high levels of dimensional stability over their lifetimes. To better understand the mechanisms for dimensional instability, a novel series of tests were carried out at Rutherford Appleton Laboratory on a breadboard high-stability optical bench structure. Goals of the testing were to assess the relative stability of a pair of reference surfaces and to determine the contributions of various structural elements and joints to dimensional instability. The breadboard was subject to an intensive environmental test campaign that included thermal cycling under vacuum and random vibration testing. Metrology was performed throughout the campaign to assess the dimensional stability response to the various environmental loads. The metrology requirement was challenging, with measurements of micron-level displacement and arc-second-level tilt over 1-meter distances being necessary in situ during environmental testing. This issue was resolved using a combination of techniques: a contacting coordinate measurement machine, laser interferometry, and optical autocollimation. The greatest levels of instability were produced by random vibration testing, though evidence of a bedding-in process implies that vibratory conditioning could be used to improve stability.

I. Introduction

TYPICAL space-based optical systems use two or more optical components and a focal plane. If the location of the detector's active surface deviates significantly from this focal plane, the resulting image will be out of focus. Similarly, there are ideal positions for the optical components, deviations from which will cause aberrations and degrade performance. The degree to which performance is compromised by relative movements of the optical elements, although depending on the particular details of the system, can be difficult to determine by numerical methods. Given that each element can move relative to the others in 6 degrees of freedom, a large number of scenarios are possible. This issue is usually tackled by attributing positional tolerances to each component, with tolerance values being determined by an optical sensitivity analysis. Obtaining adequate optical performances from visible-wavelength Earth-observation cameras in the 1 m resolution class can typically result in positional tolerances on optical components of under 10 μm and angular tolerances of under 10 arc seconds.

Although these levels are easily achievable under laboratory conditions during an initial alignment process, maintaining them through a project's assembly, integration, verification, launch, and on-orbit phases can be a challenge. There are a number of cases in the literature in which costly stability failures have been induced by alignment and verification activities and, doubtless, more that are not in the literature. For instance, the flight model of the Mars Observer camera suffered a failure during random vibration testing [1]. The cause of the failure was found to be a bonded joint, and the problem was rectified with retrofitted joint strengthening. A model of the TopSat primary mirror mount suffered a gross failure under vibration early in the program, requiring a mount redesign and a short program to verify the stability of the new system. The final design included retrofitted dowel pins to hold the mount in position. Even so, mirror deformations were observed. Alignment problems due to random vibration led to reinforcement of joints with higher-strength bolts and adhesives on the medium-sized aperture camera for the Malaysian RazakSAT [2]. Skullney et al. [3] report structural "deflections somewhat higher than anticipated" as a result of static testing on the MSX ballistic missile tracking satellite. This is a large structure, composed mainly of carbon-fiber-reinforced polymer (CFRP) struts with titanium end fittings. The results were attributed to interfacial slipping.

Received 23 April 2008; revision received 28 August 2008; accepted for publication 9 September 2008.

*Space Science and Technology Department.
†School of Engineering Sciences.

II. Background

There are two main areas in which stability can be compromised in a structure: within single structural elements or at interfaces. Understanding material properties is the key to achieving stability in single structural elements. The first material property of interest is thermal expansivity, commonly referred to in terms of the material's coefficient of thermal expansion (CTE). It is unlikely that a structure's temperature will remain constant from optical alignment to on-orbit operations or even during image acquisition periods (because large amounts of heat are typically generated around the focal plane during imaging). There are materials that have been available for some time that can be used to build structures with a near-zero CTE over its likely operating range. These include the invar family of alloys, CFRP, and more exotic materials such as glass ceramics, carbon-fiber-reinforced carbon, and silicon carbide.

When the CTE is low enough, other material properties become more important in defining the limits of stability. Although it is relatively easy to design a CFRP structure with a low CTE (i.e., below about 1 ppm/°C), the matrix polymer is typically hygroscopic and will produce dimensional instabilities in tens of parts per million when transferred from a humid laboratory environment to vacuum. Material stiffness is also a concern: the structure must be stiff enough that the optical elements it supports do not move significantly between alignment in a 1 g environment and operation in free fall: a requirement sometimes termed *gravity release*. Material response to thermal cycling may be an issue. Some materials, such as Zerodur glass ceramic, exhibit path dependency, rate dependency, and hysteresis in thermal expansivity [4].

The hygrothermal and stiffness aspects of material dimensional stability have generally been well addressed over the years, and now other factors often limit what is achievable. Some possibly less well understood mechanisms for instability are yield and creep in the microstrain region. The term *microyield strength* appears in the literature to have several definitions, though it is most commonly taken to mean the stress at which 1 ppm permanent yield is seen (as opposed to the 2000 ppm usually used to define *yield strength*). According to Marschall and Maringer [5], the mechanisms for microyield vary from material to material and can be strongly dependent on the history of the material. In metals, dislocation movements are to blame, whereas in composites, transverse microcrack (cracks in the polymer matrix, normal to the load direction) initiation and propagation can cause problems at this level [6]. Suffice it to say, microyield strength can be significantly lower than the stress levels that would typically be of concern for structural integrity and problematic for the designer of stable structures.

Time-dependent strain, or creep, is also possible in structures that have some inherent residual stresses (i.e., preloads). In materials such as epoxy adhesives and composite matrices, a viscoelastic/viscoplastic analytical approach can give good creep and microyield predictions [6,7], providing material data is sufficient. Cyclic loading introduces a new problem. For metals, cyclic plasticity can be analyzed with one of several strain-hardening models [8], for which the success is again dependent on the availability of the correct material data. Cyclic loading in composites has been well studied in the realm on thermal cycling [9,10] and even moisture cycling. Nairn [11] notes that there is, however, a fundamental difference between the biaxial loading seen under these conditions and the uniaxial loading that would typically be seen in a member subject to bending due to vibratory excitation. In this case, there appears to be very little in the literature of relevance to dimensional stability. Asymmetric cyclic loading introduces the additional possibility of material ratcheting, resulting in even greater levels of instability.

The other main area in which instabilities can occur is at joints. The two main joining methods of interest are adhesive bonding and threaded fastening. Adhesive bonding is widely used in stable optical structures. In structures with glass optics, it is really the only way to make the connection to mounting features (which are usually metallic). Apart from hygrothermal expansivities, a significant feature of many adhesives is shrinkage during cure. This can be somewhat reduced by loading it with glass beads. The ultraviolet-curing class of adhesives offers good advantages here [12], but application of the light may be difficult. Some aspects of bonded joint stability have been studied in the literature (for instance, creep in lightly loaded epoxy joints [13]), though information is limited.

Many optical structures also rely on bolted joint technology, providing another potential source of instability. They are often used at a number of locations in an optical system, allowing easy assembly (and disassembly if required) of components as well as providing some scope for adjustment and alignment of optical parts. The state-of-the-art understanding of the mechanics of bolted joints is primitive in areas, possibly hindered by the use of engineering rules of thumb and approximations. In particular, there appears to be virtually no literature on the dimensional stability aspects. Baylis [14,15] performed a number of useful static friction tests on material pairs commonly used in space structures, determining their slip coefficients. His results provide a good basis for design guidelines for bolted joints to prevent gross slipping. An interesting finding of his was that the slip coefficient under dynamic loading was higher than under static loading.

Another possible mechanism for joint instability is microslip. This is when part of the faying interface of a joint slips, but not all. Under shear loading, those regions of the joint under the lowest compressive pressure will logically slip first, with the highest-loaded regions slipping last. This phenomenon has been the subject of a long-running study at Sandia National Laboratories [16] with respect to prediction of structural damping characteristics. It may also produce permanent slippage at levels that are of interest for stability, and ratcheting of the joint under asymmetric loading may amplify these effects.

There are several ways to improve stability at jointed interfaces. Some have already been mentioned: add dowel pins, use adhesive as well as bolts, and use bolts with a higher preload. The first two of these may preclude disassembly or realignment if necessary. In addition, the drilling and reaming of dowel holes in situ in an aligned optical system presents a number of risks: debris causing contamination, loss of alignment, and the potential for accidental damage to expensive optics. Other ideas include lapping of faying surfaces and roughening, though this may be counterproductive in terms of preload loss due to embedding or plastic deformation in contacting asperities. In any case, these methods have not previously been the subject of rigorous study with respect to stability, and their relative merits are anecdotal.

There are a number of environmental conditions that are responsible for stability-challenging loads. During the assembly process, subsequent operations may disturb the alignment of already-assembled parts. Transport and handling events may cause problems. Gravity release and a possibly changing gravity vector due to alignment taking place in different orientations is an issue. Thermal and hygral changes during this period may cause problems. Vacuum, thermal cycling and atomic oxygen in low Earth orbit (LEO) are a problem after launch. During launch, dynamic loading is applied through aeroacoustic excitation at transonic speeds, reflected engine noise from the launch pad, and stage-separation shocks. Often, the qualification testing of instruments for thermal cycling and vibration is substantially more harsh than the launch and operational conditions. In the case of vibration testing, it is because it is difficult to predict the exact loads at the interface to the optical structure. Thus, an envelope is usually used that covers a range of possible events over a large frequency range, with a large margin to reflect the uncertainties involved. This means that it can often be these ground tests that are the biggest threat to stability.

Stability testing of optical bench structures is an important aspect of their development. With insufficient metrology, misalignments of optical components following environmental loading will be witnessed simply with a degradation in image quality or a change in interferometric response, without providing useful information on which part of the structure was responsible and to what degree. Metrology, either in situ or directly before and after loading, is required to assess this so that mitigating strategies can be employed. Conversely, a good degree of confidence in the likely levels of instability in a particular structural design can be fed back to impose requirements on the optical design early in the program.

Bespoke stability testing of optical bench structures has been performed a number of ways. For the TopSat mission [17], a coordinate measurement machine (CMM) with a contacting probe was used to measure the positions of highly accurate spherical tooling balls attached around the structure before and after environmental testing. Theodolites were used on Ball Aerospace's Quickbird camera structure [18]. Stability tests during thermal excursions in vacuum were performed by Giaretto et al. [19] using capacitative sensors that were accurate to 1 μm and by Cabeza and Pradier [20] using interferometric cavities inside the test chamber. Coordinate measurement of reference points on a breadboard structure was also used by Di Carlo and Usinger [21] for testing over a temperature range in air.

The aim of the present study is twofold: First, it is to assess the stability of a conventionally constructed optics bench under a number of environmental conditions by test and observation. Second, it is to assess several methods for making these measurements, in terms of accuracy and ease of use.

To satisfy the first of these, a specific goal is to quantify movements between a pair of reference surfaces within the structure, each composed of a dummy mass representing a major optical component. The degrees of freedom of importance are relative axial displacement and relative rotations about the two axes orthogonal to the axial direction. When movements of significance are observed, a secondary goal is to assess, as far as possible, which location(s) in the structure are responsible.

Three primary metrology techniques were used to assess stability. The first was in situ laser interferometry. The second was optical

autocollimation to measure tilts. The third was before and after CMM testing.

III. Test Structure

The optical bench structure has two primary parts: a stiff bulkhead panel and a large tube. The bulkhead panel is a sandwich structure with a honeycomb core and CFRP face skins. The tube is also of CFRP construction, with stiffening devices added at critical locations. An iterative design/analysis approach was taken, and so the final design was fairly well optimized for strength and stiffness. The structure was designed to accommodate optics for a Cassegrain telescope with an aperture of about 0.5 m. Dummy masses were used to represent the optical components and focal plane assembly. The layout of the optical bench is shown schematically in Fig. 1. Two reference planes of interest were defined (RP1 and RP2), one on each of the main dummy optics.

IV. Test Conditions

The assembly sequence is broadly the same as would be used for a flight instrument, though without the moisture absorption precautions. The approach is to sequentially lock out the degrees of freedom of the optical parts. Thus, RP1 is fixed, then RP2 is fixed with respect to RP1, then the focal plane assembly is fixed with respect to the optics.

RP2 was aligned with the breadboard pointing vertically. An optical autocollimator was used to align a flat mirror bonded to the center of RP1 with a flat reflective surface on RP2 to within several arc minutes in either direction. Part of the fixation process for RP2 involved the in situ drilling and reaming of dowel holes and the fitting of dowel pins (there are 12 pins in this part of the assembly). This cannot be done until RP2 is aligned. Therefore, one of the tests was to monitor the stability of RP2 with respect to RP1 during doweling operations.

The gravity release test was performed by assessing the relative alignment of the reference planes while pointing both vertically and horizontally. The test program relied on the use of facilities that were not all available on one site. After being built at Rutherford Appleton Laboratory (RAL), the breadboard was transported by road to the National Physical Laboratory in Teddington, England, 3 times for metrology, and once to Astrium in Stevenage, England, for vibration testing.

For transport, the breadboard was mounted on a frame within a large transport box via antishock mounts. The breadboard was light enough to be easily lifted by two people into and out of the box.

It is possible that critical alignments can change over time with no external forces applied, due to stress relaxation within materials, as well as creep in parts under load. This program did not allow for long periods of metrology, though stability was assessed over periods of up to a week following alignment operations.

The model was subject to random vibration testing in three directions. As no specific launcher or bus had been chosen, a generic qualification random power spectral density (PSD) curve was determined from [22], the ESA standard for structural testing. The levels used for random vibration testing gave 9.98 *g*rms in the out-of-plane direction (*Y* in Fig. 1) and 6.43 *g*rms in the in-plane directions (*X* and *Z*).

Testing was performed in the RAL space test chamber for a period of just over a week. During this period, the breadboard was continually under vacuum and was subject to two thermal cycles between -10 and $+30$°C with various plateaus at constant temperature to represent the expected on-orbit thermal environment.

V. Metrology

A CMM at the National Physical Laboratory was used to assess structural movements. This is a machine that uses a highly accurate contacting probe to measure the locations points on the structure. Measurements were made at three inspection points: before vibration, between vibration and thermal vacuum testing, and after thermal vacuum testing.

To ensure that common points could be measured each time, silicon nitride tooling balls with a very high sphericity were attached around the structure. Epoxy was used to bond a washer to the structure at each point of interest, and then each washer was used as a seat for bonding the tooling ball (see Fig. 2). During metrology, a number of points were probed around the surface of each ball, and its center was determined from a best-fit approach.

For each set of measurements, the structure was mounted on a stable granite bench and given time to thermally stabilize. Six sets of measurements were made for the center position of each ball and the average result was used.

A two-axis autocollimator was used to measure relative tilts between RP1 and RP2. Flat reflectors were located at both reference planes for this. Measurements were manually recorded, again with five readings being taken for each. A large number of measurements were made between the initial alignment and the final tests, so that a

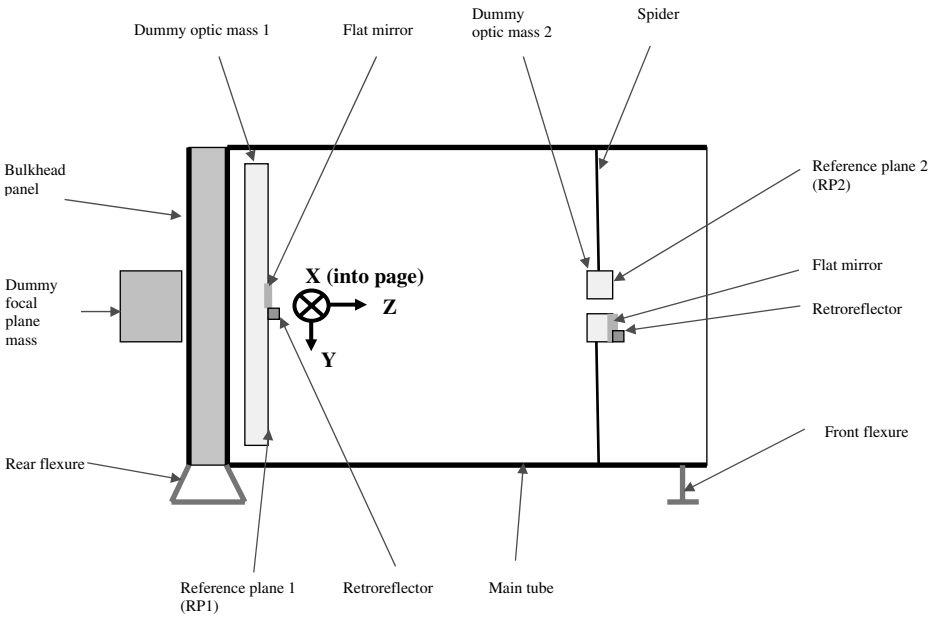

Fig. 1 Schematic cross-sectional layout of breadboard optics bench.

Fig. 2 Typical tooling-ball attachment.

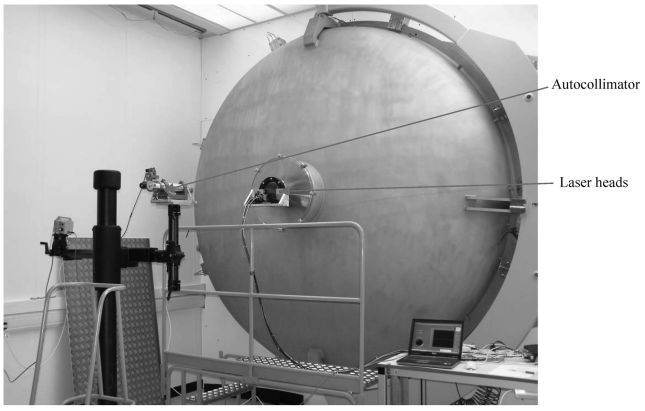

Fig. 3 Thermal vacuum test chamber.

movement timeline could be established. During vibration testing, measurements were made between each major shake. During thermal vacuum testing, the device was mounted outside a window in the test chamber, allowing measurements during testing. For the gravity release test, a 45 deg fold mirror was used to take measurements when the breadboard optical axis was pointing vertically.

An off-the-shelf Renishaw RLE-10 laser metrology system was used to measure axial displacement of RP2 relative to RP1. This system makes use of a pair of fiber-fed interferometer heads. Beam return from the target surface is done by retroreflection, which avoids difficulties in aligning flat mirrors on the test item. The corner-cube retroreflectors were solid BK7 glass, mounted on bespoke invar fixtures. One was located at RP1 (with the beams passing through the central hole in RP2), and the other was located on RP2. The device has a resolution of 79 nm. Attachment of these was done with a thin controlled epoxy bond.

This system was used for observing axial movements between RP1 and RP2 during thermal vacuum testing. The breadboard was mounted within the test chamber, aligned with the boresight pointing through a small optical quality vacuum window at one end. The pair of laser heads was mounted via a stiff fixture to the outside of the window flange, as shown in Fig. 3. With this arrangement, any errors induced due to the CTEs of the retroreflectors, as well as refractive index changes, would be common-mode errors.

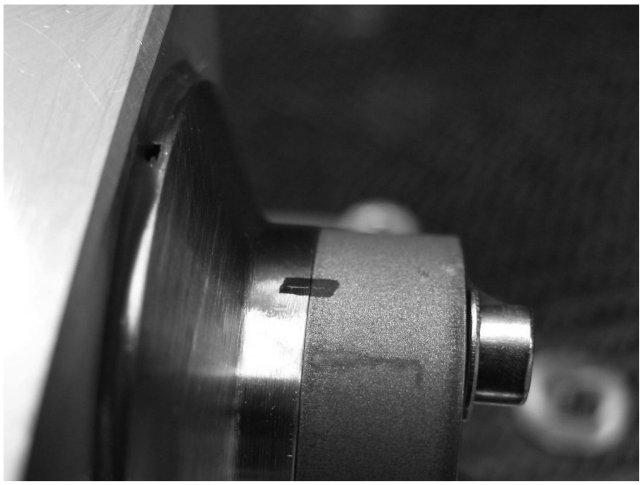

Fig. 4 Scribe marks.

Scribe marks were made across bolted interfaces after they had been locked. The marks were made over black vacuum-compatible felt-tip marker, as shown in Fig. 4. They were used to indicate whether gross slipping had occurred at these interfaces under vibration. Table 1 summarizes the metrology techniques used at various stages.

VI. Test Instrumentation

The autocollimator was a two-axis Taylor–Hobson model TA51. The reflectors used for autocollimator measurements were flat 50-mm-diam fused silica mirrors with an aluminum coating, supplied by Thorlabs.

The laser interferometer system comprised a Renishaw RLU10-A3-A3 dual-axis laser unit, with a pair of RLD10-A3-R0 detector heads mounted on a bespoke rigid fixture. The retroreflectors were 12.7-mm-diam parts supplied by Edmund Optics and made from BK7 glass with a silver coating and black overpaint. Data acquisition was performed by a National Instruments multifunction universal serial bus data acquisition card and recorded with National Instruments LabVIEW.

The CMM used for tooling-ball measurement at the National Physical Laboratory was a Leitz PMM-C 12.10.6 CMM. The tooling balls were silicon nitride balls of 10 ± 0.001 mm diameter provided by Precision Ball and Gauge. Vibration testing was conducted at Astrium's test facility in Stevenage, England, U.K. The shaker was a Ling Electronics C340, with an M&P vibration controller and D.J. Birchall charge amplifiers. Accelerometers were Endevco 224, 226, and 228 s. The thermal vacuum test chamber used was RAL's 3-m-diam space test chamber. Type-*T* thermocouples were used for temperature measurement.

Table 1 Test and metrology matrix

	CMM	Autocollimator	Laser Interferometer	Scribe Marks
Assembly	——	X	——	——
Gravity release	——	X	——	——
Transport/Handling	X[a]	X	——	——
Time	——	X	——	——
Vibration	X	X	——	X
Thermal vacuum	X	X	X	——

[a]The CMM measurements were only intended for assessing vibration and thermal vacuum movement, though transport of the test item was required to the CMM test facility.

VII. Test Procedures

The gravity release test was performed using the following basic procedure:

1) With the breadboard pointing vertically, use the autocollimator to measure the relative angle between the RP1 and RP2 reflectors about two axes. This requires a 45 deg fold mirror, as the autocollimator is mounted horizontally.

2) Point the breadboard horizontally.

3) Realign the autocollimator to ensure that reflections from both RP1 and RP2 are clearly visible; no fold mirror is now required.

4) Perform a second relative angle measurement.

The effects of adding dowel pins were assessed with the following procedure:

1) With the breadboard pointing horizontally, align the autocollimator to ensure that reflections from both RP1 and RP2 are clearly visible.

2) Fix the hole drilling location jig to the joint of interest.

3) Make an autocollimator measurement.

4) Drill the dowel holes in stages, using small increments in drill diameter to reach the correct hole size for reaming, then ream them to the final size.

5) Make an autocollimator measurement.

6) Remove the jig and fit the dowel pins.

7) Make a final autocollimator measurement.

Transport and handling were assessed with the following procedure (all measurements made with the breadboard pointing horizontally):

1) Make an autocollimator measurement.

2) Perform the transport/handling task.

3) Realign the autocollimator and perform a second measurement.

The effects of time were assessed with the following procedure:

1) Make an autocollimator measurement.

2) Leave the breadboard and autocollimator alone for a week in a temperature-controlled environment (schedule pressures prevented a longer duration being used).

3) Perform a second autocollimator measurement.

The vibration testing procedure is summarized as follows:

1) Transport the breadboard to the CMM facility. Once mounted on the CMM bed, allow the breadboard 24 h to thermally stabilize.

2) Perform initial CMM measurements.

3) Transport the breadboard to the vibration test facility and fit accelerometers.

4) Mount the breadboard on the shaker for testing in the first axis. Perform control checks.

5) Perform autocollimator measurements.

6) Perform the series of shakes as outlined in Table 2. Make autocollimator measurements between each individual shake.

7) Repeat steps 4–6 in the remaining two axes.

8) Transport the breadboard to the CMM facility. Once mounted on the CMM bed, allow the breadboard 24 h to thermally stabilize.

9) Perform final CMM measurements.

The thermal vacuum testing is summarized as follows:

1) Transport the breadboard to the CMM facility. Once mounted on the CMM bed, allow the breadboard 24 h to thermally stabilize.

2) Perform initial CMM measurements.

3) Mount the breadboard on a test fixture in the space test chamber. Ensure that it is pointing horizontally and that both retroreflectors and both flat mirrors are visible through the chamber window. Bond thermocouple sensors to areas of interest on the structure.

4) Mount the laser interferometer heads in a stiff fixture attached to the outside of the vacuum window cell. Align the beams with the retroreflectors, taking care to avoid secondary reflections from the window surfaces.

5) Align the autocollimator through the window, again avoiding window reflections.

6) Perform autocollimator measurements and commence logging laser interferometer data every 60 s.

7) Pump out the chamber and commence thermal cycling.

8) Continue logging laser interferometer data throughout the test. Perform further autocollimator measurements at the end of each temperature soak (plateau) period.

9) Return to room temperature and let up to atmospheric pressure.

10) Stop logging laser interferometer data and make final autocollimator measurements.

11) Transport the breadboard to the CMM. Once mounted on the CMM bed, allow the breadboard 24 h to thermally stabilize.

12) Perform final CMM measurements.

Table 2 Vibration test sequence

Test	Level	Duration
Resonance search	0.5 *g*	——
Low-level random PSD	−12 dB	30 s
Low-level random PSD	−6 dB	30 s
Low-level random PSD	−6 dB	30 s
Low-level random PSD	−6 dB	30 s
Full-level random PSD	−0 dB	60 s
Resonance search	0.5 *g*	——

VIII. Results

Relative tilts between RP1 and RP2 during the assembly phase are summarized in Fig. 5. The effects of gravity release are 3–4 in. tilts about each axis. The in situ doweling operations involved drilling, reaming, and fitting of dowel pins. These had surprisingly little effect on alignment, less than 5 in. in most cases. The attachment of a drilling jig to the RP2 cell had a large (20 in.) effect, though this was recovered when the jig was removed. The fastening of the breadboard to a flat optics bench was found to induce tilts of up to 8 in., even though this was done in a nominally strain-free way. The separating and reassembly of the two primary parts of the structure (the main tube and the bulkhead panel) induced a 10 in. movement in one direction and none in the other. It was found that transport in a van to and from another facility could impose tilts of up to 10 in. The entire assembly process lasted about a month after the reference planes had been aligned and locked. It is interesting to note that following the whole assembly sequence, the net movements were kept within 5 and 10 in. about both axes. These tilts would probably have been acceptable for this type of optical system, albeit using a significant proportion of the optical tolerance budget.

During vibration testing, the series of −6 dB shakes were to assess whether extra bedding-in shakes before final locking of optic positions could be used to improve stability. Unfortunately, during the final axis shake (in the lateral side-to-side *X* direction), it was found that an M6 screw had come loose at the connection between one of the spider frames with the main tube. Some very useful results were still obtained, though. A summary is shown in Fig. 6.

The first axis was the *Y* direction, which is the out-of-plane direction and had the highest PSD levels. The movements seen after the first −6 dB shake were about 5 in. This reduced to less than 2 in. for the subsequent two −6 dB shakes. The full-level shake in this axis produced movements of 8 and 13 in.

The second axis was the *Z* direction, which is parallel to the breadboard's optical axis. Large movements of 25 and 44 in. were seen here on the first −6 dB shake, dropping to very low movements for the next two −6 dB shakes. Large movements were again seen after the full-level shake in this direction.

During the third axis runs, the loose screw was discovered during the −6 dB shakes. It was retightened for the final −0 dB shake, which saw movements of 18 in. in either direction.

It is interesting to note from the first two axes' results that induced movements appear to be dependent on power levels rather than on the duration of testing. If bedding-in vibration testing is proposed for a structure, short high-power shakes may therefore be the most effective approach.

For analysis of CMM results, the tooling balls were set up in groups of three to form six planes along the length of the breadboard model. These are shown schematically as the vertical lines in Fig. 7. Each trio had balls in the 12, 4, and 8 o'clock positions (the circles in

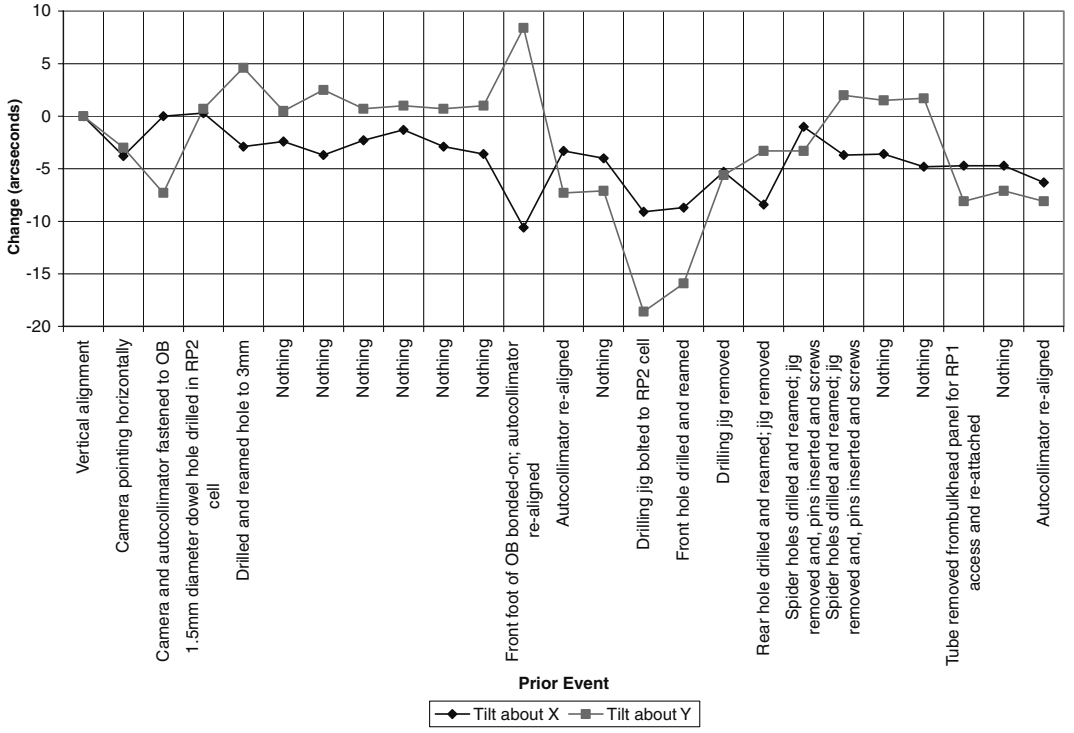

Fig. 5 Tilts during assembly (OB denotes the optics bench).

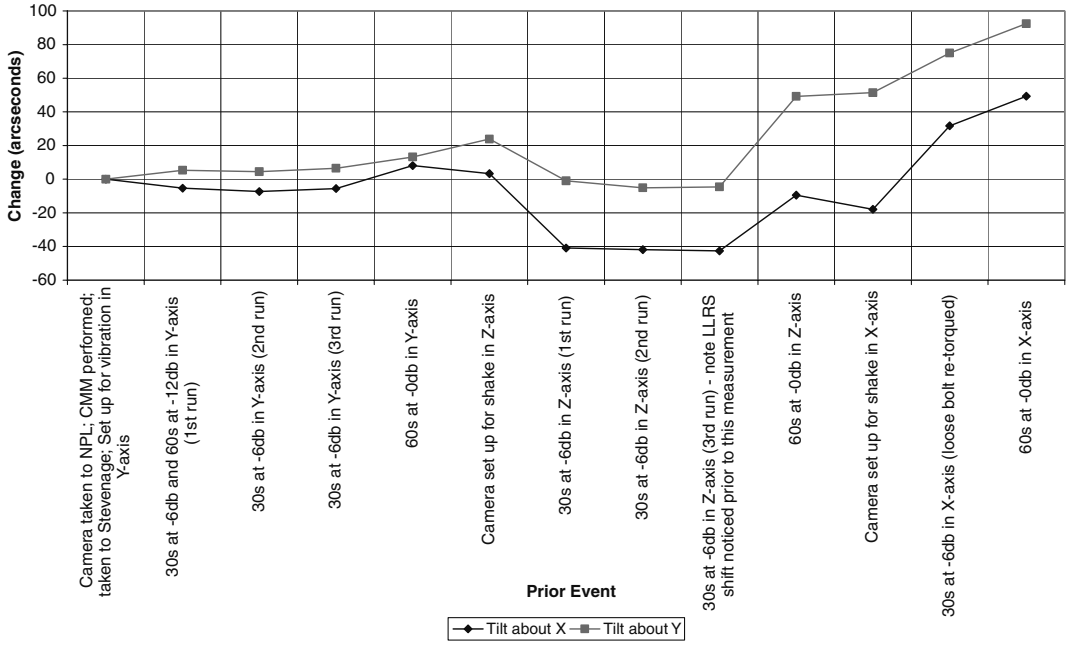

Fig. 6 Tilts during vibration testing.

Fig. 7). It was hoped that tilts and centroidal displacements along the tube could be easily assessed this way. The results show, however, that five of these planes did not behave as rigid bodies: the relative movements between in-plane balls were significant when compared with the movements of their centroids.

One of the planes was the rear skin of the bulkhead panel. It was found that the two lower balls both moved upward by about 5 μm and the upper one moved downward. This is commensurate with a permanent compressive strain in the vertical direction of 18 μm/m. There was no relative movement in the lateral direction, indicating that this effect was not a uniform in-plane expansion and therefore unlikely to be due to temperature or moisture effects.

The three balls at the front end of the tube show that this end became slightly oval, as well as tilting slightly about the lateral axis (as though the whole tube were being bent). By comparing the results at pairs of balls mounted at either end of the tube in the same clock position, the longitudinal strain in the tube was determined. This was about 25 μm (or 26 μm/m) for both the lower clock positions in a tensile sense. Some ovality was seen at the rear end of the tube as well.

Large movements were seen at RP2 (about 75 μm at the centroid) and the spiders, probably due to the loose screw. The tilt results at RP2 produced by the CMM compared reasonably well with the in situ autocollimator results (within about 10 in. in either direction).

The RP1 dummy mass behaved as a rigid body, though it did move with respect to the bulkhead panel. The net movement was equivalent to 68 in. about the lateral X axis, 10 in. about the vertical Y axis, and an axial movement at the centroid of the RP1 surface of

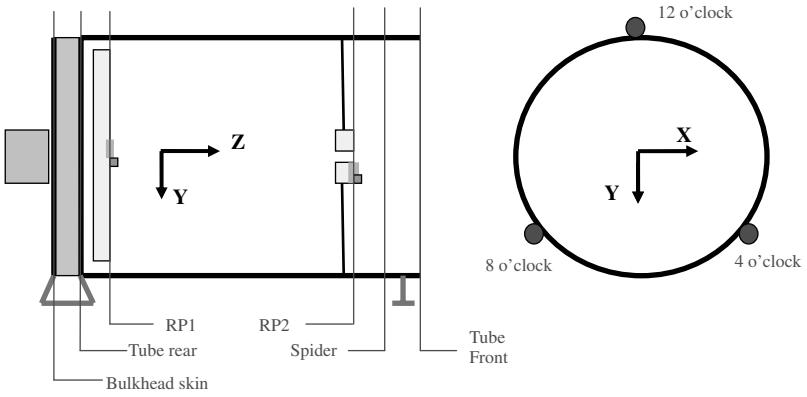

Fig. 7 CMM metrology planes and tooling-ball locations as viewed along the tube.

27 μm. This mass is attached to the bulkhead panel with a series of flexures, and there are two main interfaces in which this could have occurred: the flexure-bulkhead panel interface, which was bolted and doweled, or the flexure-RP1 dummy mass interface, which was just bolted. This is in addition to possible yield effects in the (titanium) flexure or the epoxy bond line to the dummy mass. A direct comparison between ball movements on the dummy mass and on the bulkhead panel (in adjacent positions) shows that movements occurred at all the flexure interface positions. The maximum of these was 95 μm, and occurred in one of the stiff directions for the flexure and in a direction that included a undoweled bolted joint. Tooling-ball measurements for the vibration test are shown in Table 3.

The scribe marks at the bolted interfaces were examined, though there were no signs of slipping at any interface. When the flexures were removed, however, there were visible signs of fretting at most interfaces (doweled and undoweled). This was manifested in black surface marks on both sides of the faying interface and appeared to be worst around the two lower mounts. Interestingly, the doweled interfaces showed no signs of fretting immediately around the dowel hole, but did around the screw hole (see Fig. 8. This may be indicative of microslipping.

For thermal vacuum testing, the measurements made in situ with the autocollimator and laser interferometer are summarized in Fig. 9, with the commensurate temperature profile at various points shown in Fig. 10. The thermal tests included three hot cycles and two cold cycles. Temperature control was by radiative coupling to a shroud that surrounded the structure. A significant temperature lag was seen between the outer structure and the RP1 dummy mass.

Small tilts about both axes were observed with the autocollimator throughout the tests. At the first 30°C plateau, both moved about 4 in. The largest tilts were seen during the first cooldown to −10°C and were about 11 in. about the X axis and 6 in. about Y. These values decreased for the next thermal cycle. On returning to ambient, there was no tilt about X, but there was a residual tilt about Y of 3 in. An estimate of the sensitivity of tilt to temperature, determined using the final cooling curve from 30 to 20°C, is 0.1 in./°C about X and 0.25 in./°C about Y.

Laser interferometer readings were taken every 60 s. Occasionally, one of the beams would start to lose lock on its retroreflector, and the system required resetting (resulting in a number of separate results files). If this was done relatively quickly, there was no detrimental effect on the results. However, data were lost for a period of about 12 h on the night of the third day of the test. This means that the subsequent set of results (runs 99–101 in Fig. 9) cannot be directly related to the earlier runs. The start point for the resumption of data recording was set to the final data point before lock was lost.

For the first cycle, an expansion is seen on heating from 20 to 30°C of about +3 μm. On cooling to −10°C, contractions were seen of about 14 μm. For periods of constant temperature, a gradual contraction was noticed. This is probably due to moisture expulsion. Initially, the rate was about 2 μm/day, dropping to 1 μm/day by the end of the test. The total hygral swelling expansion was estimated to be 21 μm using the manufacturer's CME (coefficient of moisture expansion) data.

The displacement-vs-temperature curves were generated using the main tube temperature as a reference. They are shown in Fig. 11. The gradient of the curves, normalized to the distance between the reference planes, is the CTE of the system. These results are quite linear over the range tested. From run 99, the average CTE on cooldown from 30 to −10°C is +0.215 ppm/°C. From run 100, the average CTE on warmup from −10 to +10°C is +0.299 ppm/°C. The difference between these is within the experimental error described in Sec. IX. For runs that have a slow-temperature change, or a dwell, the gradient is seen to vary from this, which is probably

Table 3 Summary of tooling-ball results following vibration

Plane	Tooling-ball position	ΔX, μm	ΔY, μm	ΔZ, μm
Rear skin of bulkhead panel	4 o'clock	−0.1	−4.8	0.0
	12 o'clock	−2.3	2.5	0.0
	8 o'clock	0.1	−4.8	0.0
Rear of tube	4 o'clock	21.4	−11.3	0.7
	12 o'clock	−2.6	−1.0	−3.5
	8 o'clock	−12.4	−9.2	5.0
RP1	4 o'clock	26.9	42.6	94.6
	12 o'clock	43.9	39.1	−49.0
	8 o'clock	30.6	26.7	35.3
Front of tube	4 o'clock	12.4	−34.9	23.2
	12 o'clock	4.3	−18.4	−1.2
	8 o'clock	6.4	−32.8	28.7
RP2	4 o'clock	19.6	60.1	112.3
	12 o'clock	8.8	65.0	73.4
	8 o'clock	9.4	57.2	42.0
Spider	4 o'clock	78.7	−171.6	11.7
	12 o'clock	−90.6	73.0	46.1
	8 o'clock	−157.7	−128.3	29.0

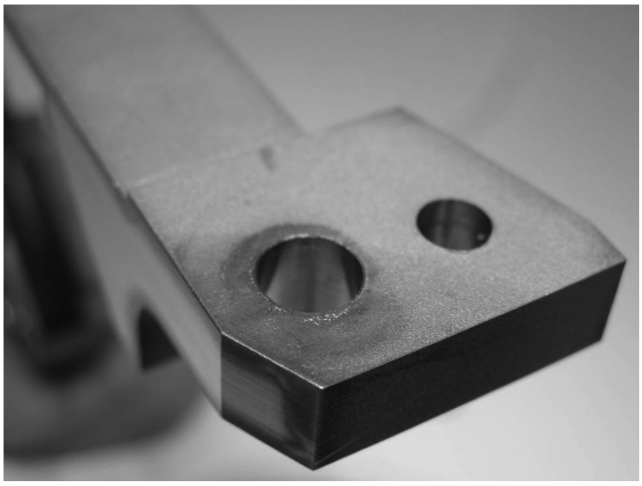

Fig. 8 Fretting around the bolt hole (left) but not the dowel hole (right).

due to moisture desorption having a greater net effect over these longer measurement periods. It should be stressed that this represents the CTE of the structural system, including flexures, spiders, dummy optic mounts, adhesive bond lines, etc., rather than simply the CTE of the main tube.

Final CMM measurements showed that residual deformations due to thermal vacuum testing were small. A fairly uniform shrinkage along the tube was noticed, probably due to the different moisture content after vacuum testing. The residual axial displacement between RP1 and RP2 was 1.6 μm, and tilts were negligible about the X axis and slightly over 3 in. about the Y axis. These again correlated well with the autocollimator results.

IX. Error Estimation

During CMM metrology, six measurements were made on each ball for each result, with the average being used for analysis. The average standard deviation of ball position was about 1.35 to 2.6 μm, and the average spread over all 6 measurements was about 3.7 to 6.9 μm. The standard deviation and spread were lower for Y (vertical) direction measurements and also lower for balls mounted at the bulkhead panel end of the breadboard. The possibility of plasticity in the ball-mounting adhesive was assessed with finite element analysis, and the effect on stability was found to be negligible for the relevant load cases.

For the autocollimator readings, the measurement technique evolved throughout testing to become more accurate. Taking measurements involved manually aligning pairs of fiducial marks and reading the angular difference from a Vernier scale. Three different people took measurements over the test period. In some test setups, the brightness of the reflected beam was very poor and/or the test rig was slightly unstable. As mentioned, for each measurement, five readings were taken of each position, and the average was used. A typical measurement has a standard deviation of about 0.5 in. and a spread of about 1.3 in.

The resolution of the laser interferometer system was set to 79 nm. There was some noise on all the results, typically with a 0.2–0.3 μm amplitude. A spurious optical-path difference is introduced within the retroreflectors as their temperature varies due to their thermal expansivity and a temperature-dependent refractive index. It was initially thought that the temperature difference between the reference planes would be negligible for most of the tests, and therefore this error would be common mode.

However, it can be seen from Fig. 10 that there is a maximum temperature difference of about 10°C. The approximate size of the optical-path difference due to this effect has been calculated to be 0.089 μm/Δ°C using the manufacturer's material data for CTE and refractive index/temperature sensitivity. Additional errors due to the CTE of the retroreflector invar mounts and adhesive bond lines are estimated at 0.011 μm/Δ°C (again, a negligible effect if both are at the same temperature). Therefore, the likely error during the cold soaks, in which the temperature difference is greatest, is about 1 μm (or 0.11 ppm/°C for the CTE). A cosine error due to the breadboard axis being slightly angled relative to the laser beams was measured and was found to be negligible.

X. Summary and Discussion

The breadboard optical bench structure showed good levels of stability during the assembly phase. The in situ fitting of dowel pins, including drilling and reaming holes, introduced only very small movements, in the region of 5 in. Gravity release was responsible for 3–4 in. tilts. The largest movements resulted from transport and handling events (10 in.), even though these were performed with great care. The net tilts at the end of the process were 5 to 10 in.,

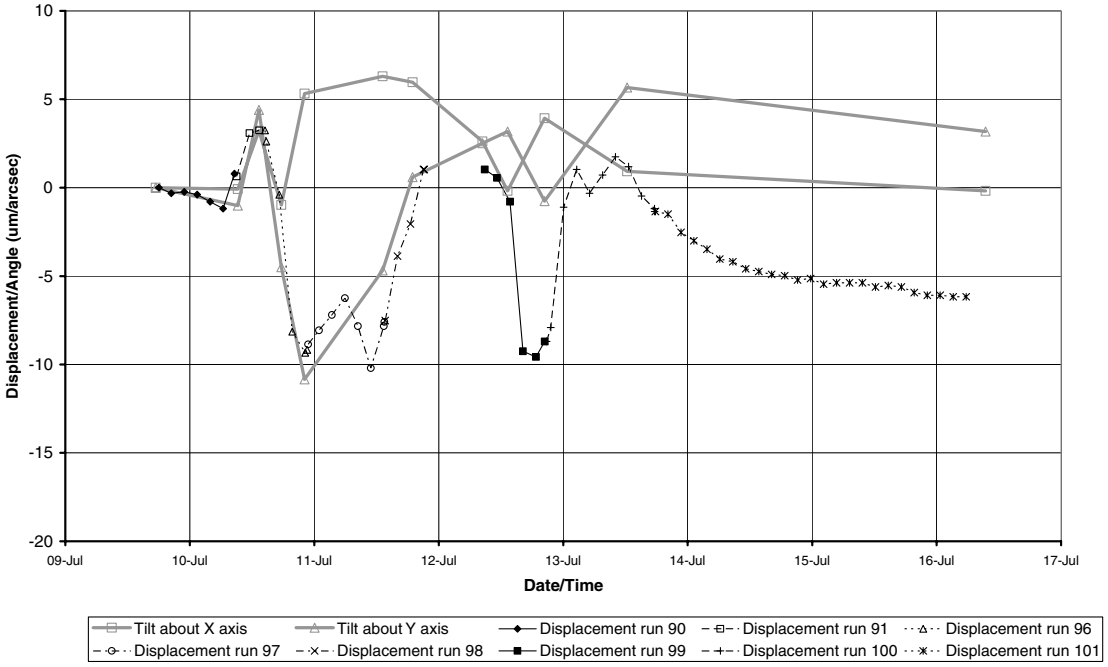

Fig. 9 Summary of laser interferometer and autocollimator measurements during thermal vacuum testing.

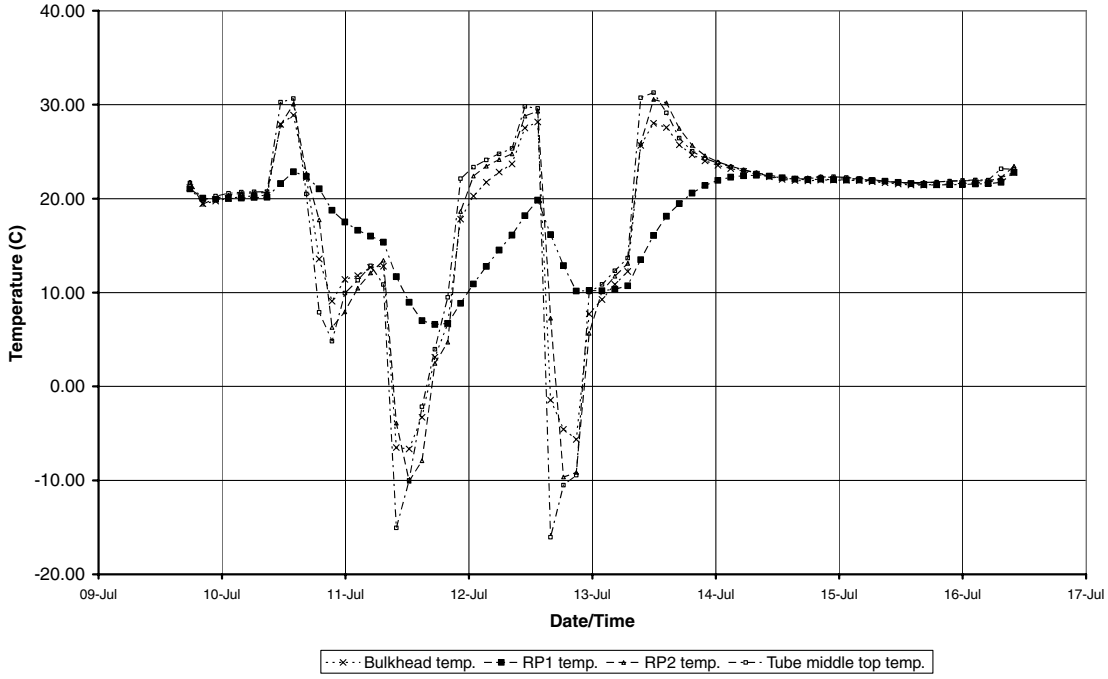

Fig. 10 Summary of breadboard temperatures.

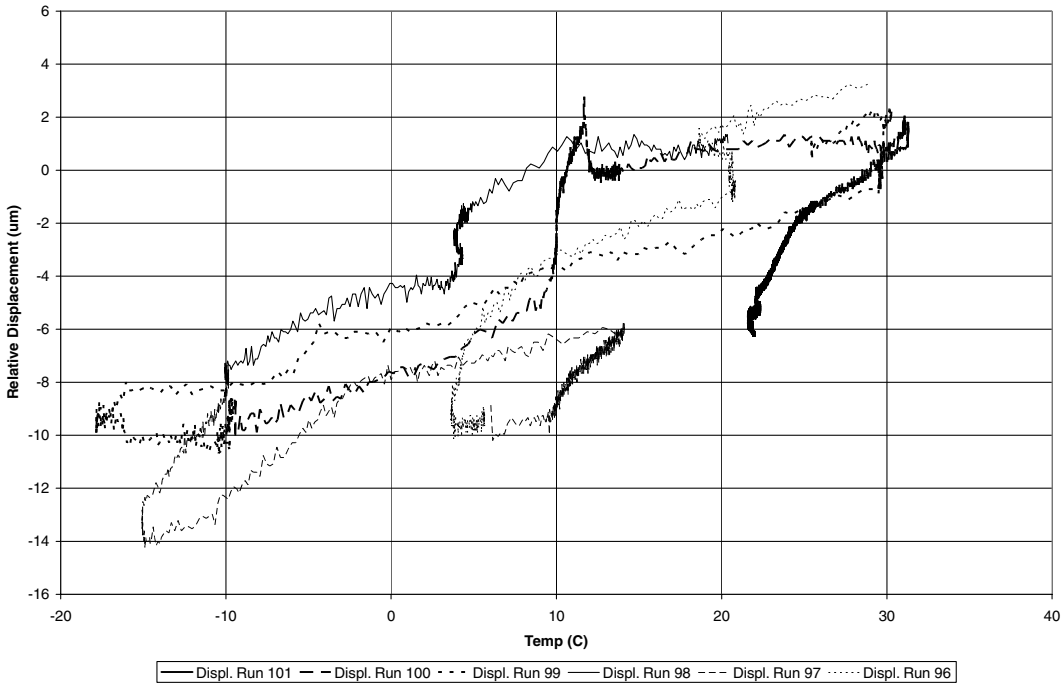

Fig. 11 Displacement vs temperature for the structure.

which probably would have been acceptable for a high-performance optical structure.

Under thermal vacuum testing, the structure was very stable, with a structural CTE of under 0.3 ppm/°C. Tilts were observed of up to 11 in., though this was at a very low temperature. If the on-orbit thermal control system were able to maintain the structure's temperature between 0 and 20°C, not an unreasonable requirement for a LEO mission, thermal expansion would be acceptable. It is recommended that if this method is to be used again, hollow retroreflectors are considered for use on reference surfaces that are at significantly different temperatures to avoid spurious optical-path differences. The effects of moisture desorption were observed during this test, but it was not part of the test plan to assess its full effect.

Large movements were seen during random vibration testing, even before the effects of the loose screw became apparent. Some of the movements appear to have occurred at jointed interfaces, whereas others occurred in the composite structure. In particular, permanent strains in the region of 15–25 μm/m were seen in the CFRP. This may be due to matrix yield or transverse microcrack initiation/propagation. On the subject of microplastic yield in CFRP, there is much discussion in the literature on the effects of low-temperature thermal cycling and hygral cycling, but little on vibration-load cases. These are necessarily different as they do not result from the quasi-uniform expansion/contraction of the composite constituents.

Interfacial movements were also observed, with a maximum of 95 μm movement seen across a flexure interface to a dummy mass. Movements in the 10 s of microns were evident at interfaces that

included dowel pins and those that did not. Evidence of fretting was seen on some doweled interfaces.

Under random vibration, there was a tendency for the structure to "bed-in." The degree of bedding-in was dependent on the amplitude of the input levels, rather than on their duration. Therefore, it is proposed that high-level short-duration bursts of random vibration could be used to condition high-stability optical bench structures before the final locking of optical component positions.

All three main metrology methods provided useful information. The autocollimator provided a relatively cheap and easy-to-use method of accurately measuring relative tilts in situ with an error of about 1 in. The CMM method gave a good indication of in-plane structural movement along the bulkhead panel skins and along the main tube, but did not provide enough information about interfacial movements. It is suggested that in the future, more tooling balls are to be used in joint areas, possibly with one ball on each interfacial component. The laser interferometer system provided an accurate in situ technique for assessing relative axial movements to submicron accuracy.

XI. Conclusions

It was found that although it is relatively easy to design and build a space optics bench composite structure that is stable during assembly, under vacuum and under thermal cycling, qualification-level random vibration testing may introduce large nonrecoverable instabilities. These are partly due to microyield in the composite structure and partly due to movements at bolted interfaces. There is little in the literature on this subject, and it is an area in which further work may help to improve the state of the art in stable structures.

The three primary metrology methods were all successful in making measurements with the accuracy required to assess stability at the micron and arc-second levels. Only the CMM method was able to provide detailed information about the specific locations and contributions of instabilities, whereas only the autocollimator was able to provide in situ measurements under a range of test conditions and continuous measurements in different locations.

References

[1] Telkamp, A. R., "Recent Developments with the Mars Observer Camera Graphite Epoxy Structure," *Proceedings of SPIE: The International Society for Optical Engineering*, Vol. 1690, 1992, pp. 180–195.
doi:10.1117/12.137994

[2] Kim, E. D., Choi, Y-W., Kang, M-S., Kim, E-E., Yang, H-S., Rasheed, A. A. A., and Arshad, A. S., "Medium Sized Aperture Camera for Earth Observation," ESA, Paper SP-554, 2004.

[3] Skullney, W. E., Kreitz, H. M., Jr., Harold, M. J., Vernon, S. R., Betenbaugh, T. M., Hartka, T. J., Persons, D. F., and Schafer, E. D., "Structural Design of the MSX Spacecraft," *Johns Hopkins APL Technical Digest*, Vol. 17, No. 1, 1996, pp. 59–74; also http://techdigest.jhuapl.edu/td1701/skullney.pdf.

[4] Jacobs, S. F., "Variable Invariables—Dimensional Stability with Time and Temperature," *Critical Reviews of Optical Science and Technology*, Vol. CR-43, Society of Photo-Optical Instrumentation Engineers, Bellingham, WA, 1992, pp. 181–204.

[5] Marschall, C. W., and Maringer, R. E., *Dimensional Instability—An Introduction*, Permagon, New York, 1977.

[6] Wolff, E. G., *Introduction to the Dimensional Stability of Composite Materials*, DEStech, Lancaster, PA, 2004.

[7] Dean, G., and Crocker, L., "The Use of Finite Element Methods for Design with Adhesives," *Measurement Good Practice Guide*, No. 48, National Physical Lab., Teddington, England, U.K., 2001.

[8] Lemaitre, J., and Chaboche, J-L., *Mechanics of Solid Materials*, Cambridge Univ. Press, Cambridge, England, U.K., 1990.

[9] Kim, R. Y., Crasto, A. S., and Schoeppner, G. A., "Dimensional Stability of Composite in a Space Thermal Environment," *Composites Science and Technology*, Vol. 60, Nos. 12–13, 2000, pp. 2601–2608.
doi:10.1016/S0266-3538(00)00052-X

[10] Abusafieh, A., Federico, D., Connell, S., Cohen, E., and Willis, P. B., "Dimensional Stability of CFRP Composites for Space Based Reflectors," *Proceedings of SPIE: The International Society for Optical Engineering*, Vol. 4444, 2001, pp. 9–16.
doi:10.1117/12.447300

[11] Nairn, J. A., "Matrix Microcracking in Composites," *Comprehensive Composite Materials*, Elsevier, New York, 2000, Ch. 2.12.

[12] Daly, J. G., and Daly, D. J., "Structural Adhesives for Bonding Optics to Metals: a Study of Optomechanical Stability," *Proceedings of SPIE: The International Society for Optical Engineering*, Vol. 4444, 2002, pp. 177–184.
doi:10.1117/12.447299

[13] Patterson, S. R., Badami, V. G., Lawton, K. M., and Tajbakhsh, H., "The Dimensional Stability of Lightly-Loaded Epoxy Joints," Lawrence Livermore National Lab. Rept. UCRL-JC-130589, Livermore, CA, 1998; also https://e-reports-ext.llnl.gov/pdf/235105.pdf.

[14] Baylis, R. J., "Slip Coefficients for Shear Joints," *Advanced Structural Materials Workshop*, ESA Paper WPP-004, 1988.

[15] Baylis, R. J., "Slip Coefficients for Shear Joints: The Effects of Dynamic Loading and Surface Treatment," ESA Paper SP-303, 1990.

[16] Lobitz, D. W., Gregory, D. L., and Smallwood, D. O., "Comparison of Finite Element Predictions to Measurements from the Sandia Microslip Experiment," *International Modal Analysis*, Vol. 2, No. 4359, 2001.

[17] Greenway, P., Tosh, I., Morris, N., "Development of the TopSat Camera," ESA, Paper SP-554, 2004.

[18] Figoski, J. W., "Alignment and Test Results of the Quickbird Telescope Using the Ball Optical Systems Test Facility," *Proceedings of SPIE: The International Society for Optical Engineering*, Vol. 3785, 1999, pp. 99–108.
doi:10.1117/12.367607

[19] Giaretto, V., Miraldi, E., Ruscica, G., Cabiati, F., and Dosio, D., "The Dimensional Stability of a CFRP Structure Probed with Sub-Millimetre Accuracy in Varying External Conditions," ESA Paper SP-386, 1996.

[20] Cabeza, I., and Pradier, A., "Dimensional Stability Verification of an Optical Bench for Space Applications Under Thermal-Vacuum Environment," ESA Paper SP-386, 1996.

[21] Di Carlo, A., and Usinger, R., "Development of a Dimensionally Stable CFRP Structure for Supporting Optical Instruments in a Laser Communication Device," *1st CEAS European Air and Space Conference* [CD-ROM], German Society for Aeronautics and Astronautics, Bonn, Germany, 10–13 Sept. 2007.

[22] "Space Engineering—Testing," ESA, European Space Research and Technology Centre, Rept. ECSS-E-10-03A, Noordwijk, The Netherlands, 2002.

J. Wei
Associate Editor